Article

pubs.acs.org/JPCC

¹ Unexpected Role of the Ru(II) Orbital and Spin Contribution on ² Photoinduced Ligand Exchange: New Mechanism To Access the ³ Photodynamic Therapy Window

- ⁴ Lauren M. Loftus, [†] Kathlyn F. Al-Afyouni, [†] Thomas N. Rohrabaugh, Jr., [†] Judith C. Gallucci, [†] Curtis E. Moore, [†] Jeffrey J. Rack, **, [‡] and Claudia Turro**, [†]
- 6 †Department of Chemistry and Biochemistry, The Ohio State University, Columbus, Ohio 43210, United States
- ⁷Department of Chemistry and Chemical Biology, University of New Mexico, Albuquerque, New Mexico 87131, United States
- 8 Supporting Information

10

11

12

13

15

16

17

18

19

20

21

23

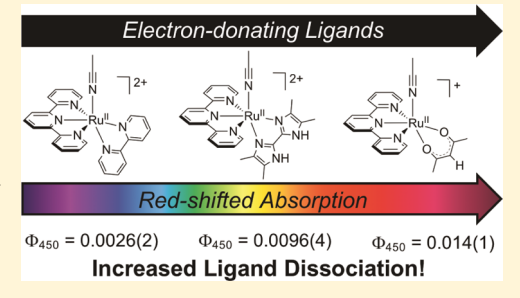
24

2.5

26

27

ABSTRACT: A series of 12 Ru(II) complexes of the type $[Ru(tpy)(L)-(CH_3CN)]^{n+}$, **1–12**, containing the tridentate tpy ligand (tpy = 2,2':6',2"-terpyridine) and various bidentate ancillary ligands, L, were synthesized and evaluated for their ability to photodissociate CH_3CN , a model for nitrile-containing drugs. Although the bidentate ligands chosen display a similar degree of steric bulk around the metal center in the ground state, the photosubstitution efficiencies of **1–12** vary by approximately an order of magnitude. The complexes containing the most electron-donating bidentate ligands, **8–11**, exhibit the larger quantum yield values for ligand exchange in water. Complexes **8–11** also possess the smallest energy gap between the ground state and the lowest energy metal-to-ligand charge-transfer (${}^{3}MLCT$)



excited state, and density functional theory calculations show that a large degree of the ligand character is present in their highest occupied molecular orbitals (HOMOs) and in their 3MLCT excited states. These results show that ligand mixing affects the π -back-bonding ability of the metal center in the excited state, increasing the quantum yields of nitrile ligand dissociation. Linear relationships were observed between the quantum yield of ligand dissociation and both the Mulliken spin density on the metal center in the excited state and the percent of the Ru(d) character in the ground-state HOMO. These findings, driven by the presence of π -donating ancillary ligands that enhance excited-state reactivity, can be used to design new complexes with greater quantum yields for the release of nitrile-containing drugs and biological probes without affecting their stability in the dark.

8 INTRODUCTION

29 Ruthenium polypyridyl complexes have long been of interest 30 for use in a wide range of applications, including solar energy 31 conversion, water oxidation catalysis, molecular switches, 32 biological sensors, and photoredox catalysis, among others. 1-26 33 The wide range of applications of these types of complexes is 34 due to their unique and highly tunable excited-state properties, 35 typically characterized by relatively strong absorption through-36 out the visible range, intense emission, and long-lived triplet 37 metal-to-ligand charge-transfer (³MLCT) excited states. In 38 these complexes, the properties of the ³MLCT states can be 39 readily tuned by synthetic modification of the ligands around 40 the metal center. 27,28 For example, previous works on 2,2'-41 bipyridine (bpy) complexes of Ru(II) showed that in many 42 cases, the emission of these complexes does not occur from a 43 "pure" ³MLCT state. Rather, density functional theory (DFT) 44 calculations suggest that bpy-based orbitals mix with the 45 Ru($d\pi$)-based singly occupied molecular orbital in the ³MLCT 46 state, resulting in a greater degree of mixing of the $\pi\pi^*$ 47 character into the ³MLCT excited state. Of the compounds 48 investigated, this effect was most pronounced in [Ru-49 $(bpy)_2(CH_3CN)_2^{2+}$ and $[Ru([9]aneS_3)(bpy)(CN)]^+$, where

[9] ane $S_3 = 1,4,7$ -trithiacyclononane. Additional modeling of 50 emission spectra of $[Ru(bpy)(L)_4]^{n+}$ and $[Ru(bpy)_2(L)_2]^{n+}$, 51 where L represents a wide variety of mono- and bidentate 52 ligands, showed that the lowest energy MLCT states of 53 complexes that absorb or emit at energies that fall within or 54 near the near-infrared (NIR) region tend to possess less 55 charge-transfer (CT) character and more ligand-based $\pi\pi^*$ 56 character. This mixing between $Ru(d\pi)$ orbitals and $bpy(\pi^*)$ 57 orbitals leads to a lower degree of the metal character in the 58 highest occupied molecular orbital (HOMO) of the ground 59 state.

Recently, the field of photochemotherapy (PCT) has 61 evolved as one potential application of polypyridyl Ru(II) 62 complexes that has very different excited-state requirements 63 than sensing and solar energy conversion. The latter requires a 64 long-lived, emissive ³MLCT state, whereas it has long been 65 postulated that efficient photoinduced ligand dissociation for 66 the release of biologically active drugs or probes with 67

Received: February 18, 2019 Revised: March 31, 2019



Complexes where n = 2

$$L = \begin{pmatrix} 1 & 2 & 3 & 4 \\ & & & & \\ & & & & \\ & & & & \\ & & & & \\ & & & & \\ & & & & \\ & & & & \\ & & & & \\ & & & & \\ & & & & \\ & & & & \\ & & & & \\ & & & & \\ & & & & \\ & & & & \\ & & & & \\ & & & & \\ & & & & \\ &$$

Complexes where n = 1

Figure 1. Schematic representation of the complex structure and the bidentate ligands, L.

68 spatiotemporal control necessitates the population of non-69 emissive, dissociative metal-centered ligand-field (³LF) 70 states. ^{32–40} Presently, much of the work in the field has 71 centered on increasing photosubstitution quantum yields by 72 introducing steric bulk pointed toward the metal, resulting in 73 distortions from the pseudo-octahedral geometry around the 74 Ru(II) center in the ground-state structure that lower the 75 energies of the ³LF excited states. ^{32,34,41–46} However, recent 76 work by our group on a series of Ru(II) complexes containing 77 tetradentate ligands related to tris(2-pyridylmethyl)amine 78 revealed that of the four complexes investigated, the only 79 one that possessed a mixed ${}^{3}MLCT/{}^{3}\pi\pi^{*}$ state as the lowest 80 energy triplet state has a quantum yield of ligand dissociation 81 that is ~five-fold greater than that of the analogous complex 82 without a heavily mixed ³MLCT state. ⁴⁷

The surprisingly wide range of photosubstitution reactivities 84 displayed by closely related types of complexes, 35,45,46,48-50 85 coupled with the desire to synthesize compounds that absorb 86 in the "photodynamic therapy (PDT) window" from 600 to 87 900 nm, 51,52 have made the rational design of Ru(II) 88 complexes that are well suited for PCT difficult to date. 89 Additionally, it has been generally believed that complexes with 90 low-energy MLCT states that could absorb in this PDT 91 window would not be able to undergo efficient ligand 92 dissociation, as the energy gap between MLCT and 93 dissociative LF states would be too large. 35-39,49,53,54

The present work focuses on the investigation of the 95 photoinduced ligand exchange of a series of relatively 96 unstrained [Ru(tpy)(L)(CH₃CN)]ⁿ⁺ complexes (Figure 1), 97 where tpy = 2,2':6',2''-terpyridine and the neutral ligands L are 98 2,2'-bipyridine (bpy, 1), 1,10-phenanthroline (phen, 2), 4,4'-99 dimethyl-2,2'-bipyridine (4,4'-Me₂bpy, 3), 4,4'-dimethoxy-100 2,2'-bipyridine (4,4'-(MeO)₂bpy, 4), 4,4'-di-tert-butyl-2,2'-101 bipyridine (4,4'-'Bu₂bpy, 5), 1H,1'H-2,2'-biimidazole (bim, 102 6), and 4,4',5,5'-tetramethyl-1H,1'H-2,2'-diimidazole 103 (Me₄bim, 7), for which n = 2, while the anionic ligands L

utilized are acetylacetonate (acac, 8), 3-chloroacetylacetonate 104 (Cl-acac, 9), 3-bromoacetylacetonate (Br-acac, 10), 2,2,6,6-105 tetramethyl-3,5-heptanedionate (thd, 11), and 1,3-diphenyl- 106 1,3-propanedione (DBM, 12), for which n = 1. Complexes 1– 107 12 exhibit a wide range of photosubstitution efficiencies, 108 despite the similarity in steric bulk afforded by the ancillary 109 ligands throughout the series. DFT provided information on 110 the excited states and bonding of 1-12, and it was used to 111 relate the calculated Mulliken spin density (MSD) on the 112 ruthenium metal center in the lowest energy triplet state with 113 the quantum yield of ligand exchange. In contrast to 114 expectation, the complexes with the lowest metal character 115 and spin density in the lowest energy triplet state are the most 116 photoactive. Importantly, counter to the commonly accepted 117 notion that complexes with low-energy ³MLCT states do not 118 possess sufficient energy to populate the dissociative ³LF states 119 and undergo ligand exchange, 35,53 and the four most active 120 complexes of the series, 8-11, exhibit the most red-shifted 121 ¹MLCT absorption maxima. ⁵⁵ These relationships can serve as ₁₂₂ a powerful tool to predict the photochemical activity of a 123 related series of analogous complexes, and shows that efficient 124 ligand photodissociation in the PDT window is attainable 125 without sacrificing thermal stability or photoreactivity. The 126 present work highlights the importance of metal/ligand orbital 127 mixing on photophysical properties and points to the 128 complexity of the excited-state reactivity of Ru(II) complexes. 129 Moreover, it reveals a new strategy for the design of ruthenium 130 complexes for the photoinduced release of therapeutics and 131 diagnostic molecular probes.

RESULTS AND DISCUSSION

Synthesis and X-ray Crystallography. Complexes 1-12 134 were synthesized from two well-known starting materials, 135 either $[Ru(tpy)Cl_3\cdot 3H_2O \text{ or the } [Ru(\eta^6-p\text{-cymene})(\mu\text{-Cl})Cl]_2$ 136 dimer to form the appropriate [Ru(p-cymene)(L)Cl] complex 137 (Supporting Information, Figures S1–S16). In both cases, the 138

139 synthetic procedures allow for the stepwise installation of the 140 ligands in a fashion that greatly reduces the formation of by 141 products and renders the desired product easily purified from 142 any homoleptic complexes formed. All complexes were 143 obtained in moderate to good yields.

The X-ray crystal structure of 4 is shown in Figure 2a and is 14s similar to that of its parent complex 1 and related 4,4'-

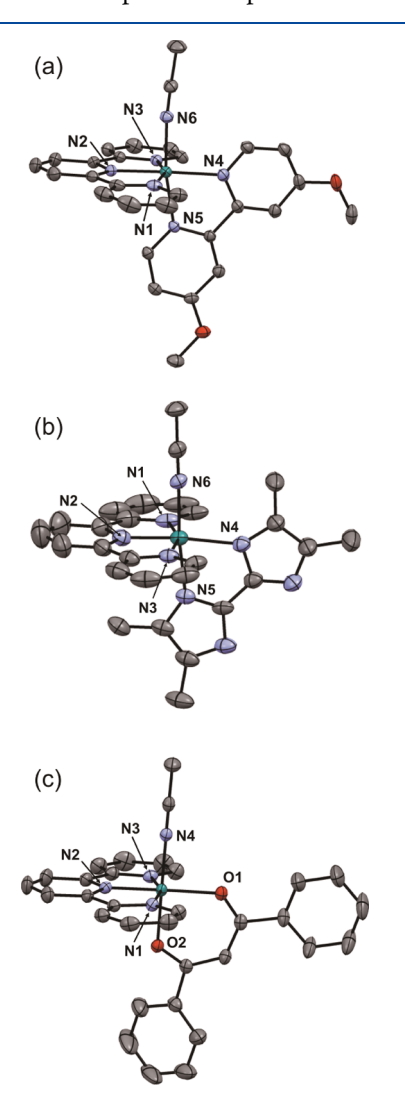


Figure 2. Oak Ridge thermal ellipsoid plots of (a) 4, (b) 7, and (c) 12 (ellipsoids drawn at 50% probability and hydrogen atoms have been omitted for clarity); Ru: cyan, N: light blue, C: gray, and O: red.

146 substituted bpy complexes (see Tables S3—S7 and references 147 therein). The similar bond lengths between 1 and 4 indicate 148 that the methoxy substituents in the 4,4′ positions of the bpy 149 ring have little influence on the overall ground-state structure

of 4 (Table 1), ⁵⁶ while the similar bite angle of the bidentate 150 th ligand and tilt angle of the CH₃CN ligand indicate a similar 151 degree of steric distortion that can be found between 1 and 4 152 (Table 1), as expected.

The X-ray crystal structure of 7 is shown in Figure 2b. 154 Despite the presence of the two methyl groups adjacent to the 155 coordinated N atoms, the Ru–N bond lengths, the bite angle 156 of the bidentate ligand, and the tilt angle of the coordinated 157 CH₃CN ligand in 7 are very similar to those observed in 1 158 (Table 1), ⁵⁶ suggesting a similar degree of steric hindrance 159 present in the ground state between the two complexes. At 160 2.118 and 2.103 Å, the Ru–N bonds to the Me₄bim ligand in 7 161 are slightly elongated compared to the Ru–N bonds in the 162 bpy-based complexes (Table 1); however, they are similar to 163 those observed in related biimidazole-containing complexes 164 without the methyl groups present and therefore are not 165 indicative of steric strain in the coordination sphere (see Table 166 S8 and references therein).

The X-ray crystal structure of 12 (Figure 2c, Table 2) is $_{168}$ to similar to that of its parent complex 8 (Tables S10–S14). $_{55}$ $_{169}$ The addition of the phenyl rings to the bidentate ligand in 12 $_{170}$ does not have a significant effect on its ground-state structure, $_{171}$ as these groups are pointed away from the metal center and do $_{172}$ not add additional steric distortion, as evidenced by the nearly $_{173}$ identical tilt angle of the CH $_{3}$ CN ligand in 12 as compared to $_{174}$ that of 8 (Table 2). It is interesting to note, however, that the $_{175}$ bite angle of the bidentate ligand in the acac-based complexes $_{176}$ is closer to ideal octahedral geometry, $_{90}$ °, than in the $_{177}$ complexes derived from bpy, $_{80}$ ° (Tables 1 and 2), $_{178}$ indicating that there should be a lesser degree of steric $_{179}$ distortion and slightly better orbital overlap present in 8–12 $_{180}$ than in 1–5.

Photochemistry. The electronic absorption spectra of 1-5 182 (Figure S17) are typical of diimine Ru(II) complexes 183 containing tpy, with a moderately intense mixed MLCT 184 transition of both Ru(d π) \rightarrow bpy/phen(π^*) and Ru(d π) \rightarrow 185 tpy(π^*) characters at ~455–458 nm and a low-energy 186 shoulder at \sim 570–585 nm that is Ru(d π) \rightarrow tpy(π *) in 187 nature (Table 3). 57,58 In these complexes, the electron 188 t3 withdrawing/donating character of the substituent in the 189 4,4'-positions of the bipyridine ligand has only a slight 190 influence on the energy of the most intense ¹MLCT transition. 191 Complexes 6 and 7 exhibit similar absorption spectra (Figure 192 S18, Table 3), with ¹MLCT transition centered at ~465 nm 193 that is $\operatorname{Ru}(\mathrm{d}\pi) \to \operatorname{tpy}(\pi^*)$ in character. However, the 194 introduction of the biimidazole-type bidentate ligand in these 195 complexes leads to more pronounced and red-shifted Ru($d\pi$) 196 \rightarrow tpy(π^*) shoulders at ~550 and 600 nm (Table 3). The 197 presence of the more electron-donating acac and electron- 198 substituted acac bidentate ligand in 8-12 destabilizes the 199 $Ru(d\pi)$ set and red-shifts the absorption into the PDT window 200

Table 1. Selected Bond Lengths (Å) and Angles (deg) in 1,56 4, and 7

| | Ru-N bond | | | | | | bidentate bite angle | |
|---|-----------|----------|----------|----------|-----------------|-----------------|----------------------|-------------------------------|
| | N1 | N2 | N3 | N4 | N5 ^a | N6 ^b | N4-Ru-N5 | CH₃CN tilt angle ^c |
| 1 | 2.063(8) | 1.953(8) | 2.077(8) | 2.062(8) | 2.038(9) | 2.03(1) | 79.2(3) | 169.8(9) |
| 4 | 2.071(2) | 1.970(2) | 2.080(2) | 2.074(2) | 2.054(2) | 2.032(2) | 78.28(8) | 173.3(2) |
| 7 | 2.067(9) | 1.945(4) | 2.064(3) | 2.118(3) | 2.103(3) | 2.023(3) | 78.5(1) | 178.4(3) |

[&]quot;Atom positioned trans to the CH₃CN ligand. "CH₃CN. "The CH₃CN tilt angle is defined as the angle from Ru–N6–C*; C* represents the carbon atom adjacent to N6 in CH₃CN (C26 in 1, C28 in 4, and C26 in 7).

Table 2. Selected Bond Lengths (Å) and Angles (deg) in 8⁵⁵ and 12

| | Ru-N bond | | | | Ru-O bond | | bidentate bite angle | |
|----|-----------|----------|----------|-----------------|-----------|------------------------|----------------------|--|
| | N1 | N2 | N3 | N4 ^a | O1 | O2 ^{<i>b</i>} | O1-Ru-O2 | CH ₃ CN tilt angle ^c |
| 8 | 2.069(2) | 1.939(1) | 2.056(2) | 2.014(2) | 2.080(1) | 2.056(1) | 91.50(6) | 177.2(2) |
| 12 | 2.063(3) | 1.945(3) | 2.070(4) | 2.015(4) | 2.078(2) | 2.037(3) | 90.8(1) | 176.7(3) |

^aCH₃CN. ^bAtom positioned trans to CH₃CN. ^cThe CH₃CN tilt angle is defined as the angle from Ru–N4–C*; C* represents the carbon atom adjacent to N4 in CH₃CN (C21 in 8 and C31 in 12).

Table 3. Photochemical, Photophysical, and Electronic Structure Data for 1-12

| | | | | | | S HOMO MSD-3ML | |
|----|--|----------------------------------|-------------------------------|-----------------------------|--------|----------------|-------|
| | $\lambda_{\rm max}/{\rm nm}~(\varepsilon/{\times}10^3~{\rm M}^{-1}~{\rm cm}^{-1})^a$ | $\lambda_{\rm em}/{\rm cm}^{-1}$ | $\Phi_{450}(\mathrm{H_2O})^c$ | $\Phi_{450}(\mathrm{Cl})^d$ | % Ru d | Ru | tpy |
| 1 | 455 (10.4) | 16Å600 | $0.0026(2)^{e}$ | 0.0062(1) | 76.3 | 0.881 | 0.909 |
| 2 | 455 (11.0) | 16Å600 | 0.0053(1) | | 76.1 | 0.878 | 0.983 |
| 3 | 456 (9.9) | 16Å100 | 0.0031(3) | 0.0049(1) | 76.1 | 0.882 | 0.989 |
| 4 | 458 (8.8), 530 (1.7), 585 (0.7) | 15Å700 | 0.0048(3) | | 73.2 | 0.870 | 1.04 |
| 5 | 455 (10.4), 515 (1.8), 570 (0.6) | 16Å100 | 0.0022(1) | | 75.8 | 0.886 | 1.07 |
| 6 | 465 (5.4), 545 (1.6), 600 (0.9) | 15Å100 | 0.0035(2) | | 74.8 | 0.882 | 1.08 |
| 7 | 468 (5.7), 555 (1.6), 620 (0.8) | 14Å600 | 0.0096(4) | | 61.2 | 0.813 | 1.06 |
| 8 | 530 (5.8) | 13Å100 | $0.014(1)^f$ | 0.026(1) | 61.3 | 0.804 | 1.05 |
| 9 | 519 (5.5) | 13Å600 | $0.018(1)^f$ | | 48.3 | 0.741 | 1.04 |
| 10 | 521 (5.4) | 13Å700 | $0.016(1)^f$ | 0.027(1) | 47.1 | 0.738 | 1.04 |
| 11 | 535 (5.9) | 13Å000 | $0.015(1)^f$ | 0.022(1) | 58.8 | 0.786 | 1.04 |
| 12 | 522 (7.4) | 13Å300 | 0.0012(1) | 0.021(1) | 58.2 | 0.785 | 1.04 |

[&]quot;Acetone. "From emission in CH₃CN at 77 K; diimine complexes are weakly emissive at 298 K and acac derivatives were weakly luminescent at 77 K. "CH₂O (<5% acetone) at 298 K. "CH₂Cl₂ with 10 mM Bu₄NCl at 298 K. "From ref 59." From ref 55.

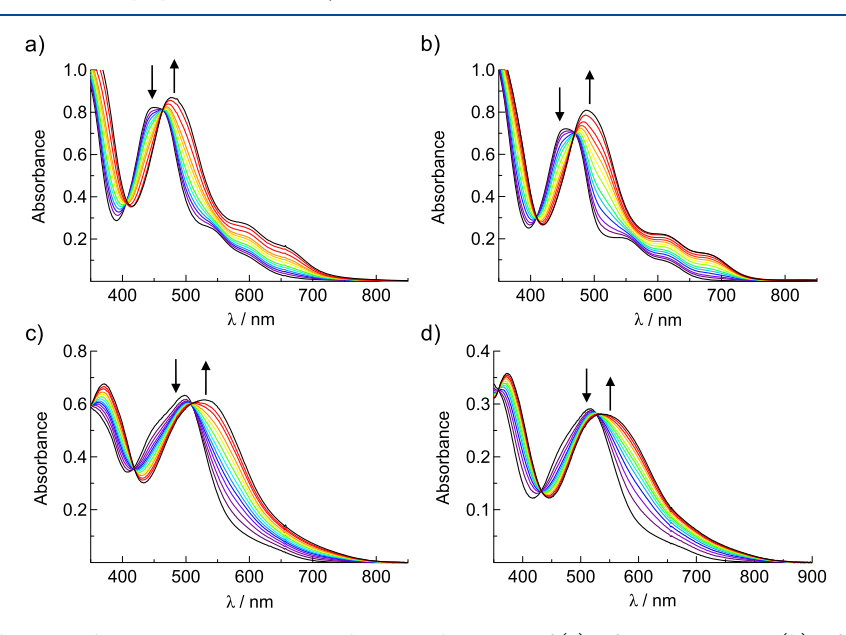


Figure 3. Changes in the electronic absorption spectra upon irradiation with 655 nm of (a) 6 from 0 to 30 min, (b) 7 from 0 to 16 min, (c) 9 from 0 to 160 s, and (d) 11 from 0 to 100 s in H_2O (<5% acetone).

201 (Figure S19), with 1 MLCT transitions between 519 and 535 202 nm and Ru(dπ) \rightarrow tpy(π*) shoulders at ~700 nm (Table 3). S5 203 Irradiation of these complexes with $\lambda_{irr} \geq 395$ nm in water 204 (<5% acetone) leads to the expected red shift of the MLCT 205 absorption as the CH₃CN ligand exchanges with the weaker-206 field OH₂ ligand and forms the respective aqua complex 207 (Figure S20). S5,59 Complexes 1–12 are stable in water (<5% 208 acetone) in the dark for at least 3 h (Figure S21). Complexes 209 6–11 are unique in that their red-shifted transitions place a 210 considerable amount of absorption in the PDT window,

allowing for efficient photodissociation using 655 nm LEDs on $_{211\,f3}$ a practical timescale (Figure 3).

Quantum yields of ligand exchange for 1–12 were measured $_{213}$ in $_{12}$ O (<5% acetone) using $\lambda_{irr}=450$ nm (Φ_{450}), and the $_{214}$ resulting values span an order of magnitude. Complex 12 $_{215}$ exhibits the lowest quantum yield, $\Phi_{450}=0.0012(1)$, and 9 $_{216}$ exhibits the highest, $\Phi_{450}=0.018(1)$ (Table 3). The quantum $_{217}$ yields for 7–11 were unexpectedly high, given their red-shifted $_{218}$ absorption spectra, while that for 12 was lower than expected, $_{219}$ given the structural similarities to its acac parent complex, 8, $_{220}$ and other acac derivatives 9–11. This large range in $_{221}$

222 photodissociation efficiency was surprising, as crystal structures 223 or DFT-optimized structures of **1–12** (Tables 1 and 2 and 224 S3–S14) show no discernible differences in the amount of 225 steric distortion around the metal center in the ground state 226 that is well known to affect the relative energy of the ³LF states 227 thought to be responsible for ligand photodissociation. ^{41,42} 228 This finding suggests that other electronic factors in either the 229 ground state or excited state may play a significant role in the 230 efficiency of photoinduced ligand exchange in this series of 231 complexes.

Ground-State Electronic Structure Calculations. In an 2.32 233 effort to understand the observed photochemical trends, 234 electronic structure calculations were undertaken. Geometry 235 optimizations for 1-12 in the singlet ground state produced 236 structures in good agreement with crystallographic data and 237 calculated $\nu(CN)$ stretches consistent with experimental values (Tables S3–S14). The electronic structure of these complexes 239 in the ground state can be described by the frontier molecular 240 orbitals, which are similar across the series (Figures S22–S24). 241 The HOMOs of 1-12 are mostly composed of Ru d character 242 with varying degrees of ligand mixing, while the lowest 243 unoccupied molecular orbitals (LUMOs) are nearly exclusively 244 localized on the tpy ligand. Representative orbital contours for 245 the HOMOs and LUMOs of complexes 2 and 8 are shown in 246 Figure 4. It is evident from Figure 4a that the HOMO of 2 is

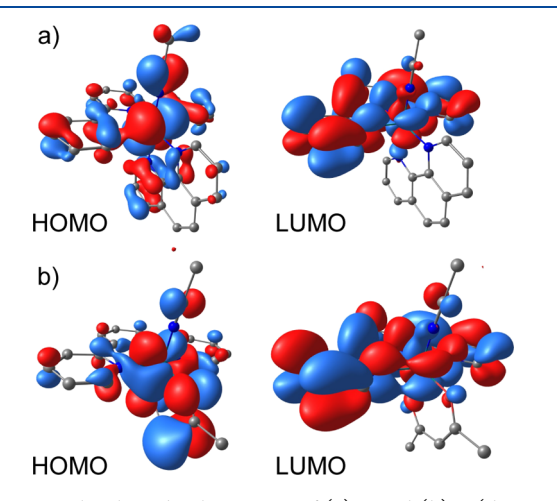


Figure 4. Molecular orbital contours of (a) 2 and (b) 8 (drawn at an isovalue of 0.02).

247 localized on the metal with little contribution from the ligands, 248 whereas Figure 4b shows extensive Ru-acac mixing leading to 249 significant localization of the HOMO of 8 on the acac ligand. 250 The LUMOs of 2 and 8 are localized on the tpy ligand. The 251 HOMOs and LUMOs of 1–12 are compared in Figures S22–252 S24, and the calculated percent contribution of the Ru d-253 orbital to the HOMO of each complex in the singlet ground 254 state, ¹GS, is listed in Table 3.

It is evident from the data presented in Table 3 that, with 256 the exception of 12, the complexes with higher quantum yields 257 of ligand exchange in water, $\Phi_{450}(H_2O)$, are calculated to 258 possess a lower amount of Ru d character in the HOMO, % 259 Ru(d). In fact, a plot of $\Phi_{450}(H_2O)$ versus % Ru(d) results in a 260 linear relationship (Figure 5), suggesting that ligand mixing in 261 the HOMO is important for efficient ligand dissociation. A 262 significant degree of the ligand character has previously been 263 shown to have a dramatic impact on the efficiency of

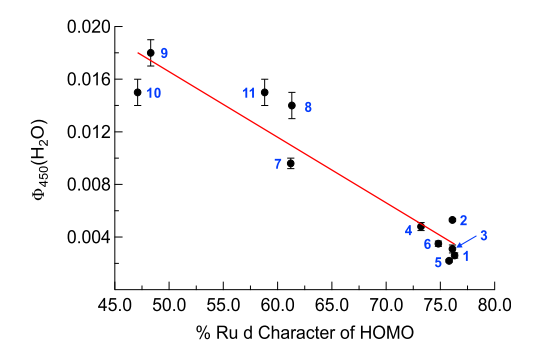


Figure 5. Plot of the measured $\Phi_{450}(H_2O)$ vs the calculated percentage of Ru d character in the ground-state HOMO of **1–11**; the data can be fit to a line with $R^2=0.90$.

photoinduced ligand dissociation of nitriles in other types of 264 polypyridyl Ru(II) complexes.⁴⁷

MSDs in the Triplet Excited State. Geometry opti- 266 mizations and vibrational frequency calculations of 1-12 were 267 also completed in the triplet excited state (Tables S3-S14). All 268 complexes show elongated Ru-N(CH₃CN) bonds in the 269 triplet excited state as compared to the ground state. MSD 270 calculations were performed to determine the spin density on 271 the Ru(II) center and to examine the nature of the triplet 272 excited state. For complexes with a ³MLCT state as the lowest 273 energy triplet state, the MSD on the Ru(II) center should 274 theoretically equal one, indicating exactly one unpaired 275 electron on the metal. Complexes with a ³LF state as the 276 lowest energy triplet state should have a spin density of two on 277 the Ru center, consistent with the presence of two unpaired 278 electrons on the metal. Any complex with a spin density on the 279 metal that is not precisely one or two suggests some degree of 280 metal/ligand mixing. For 1-12, the MSD on the Ru(II) center 281 was calculated to be less than one, with some complexes 282 exhibiting a significant amount of Ru(II) mixing with both the 283 tpy and bidentate ligands. The calculated MSD values for 1- 284 12 in the triplet state on Ru and on the tpy ligand are listed in 285 Table 3, and the values indicate that the lowest energy triplet 286 excited state is MLCT in nature with a significant amount of 287 the ligand character. Figure 6 compares the MSD values on the 288 f6 metal and the ligands of the ${}^{3}MLCT$ state of 1, 6, and 8.

A linear relationship was also found between the MSD on 290 Ru in the ³MLCT excited state and the quantum yield of 291 ligand dissociation in water for 1–11 (Figure 7). This finding 292 f7 again points to the increase in ligand exchange efficiency with a 293 decrease in Ru d character or greater metal/ligand mixing.

³MLCT Energies and Photoanation. Additionally, a 295 trend is also observed between the quantum yield for ligand 296 dissociation measured in H₂O and the emission maximum 297 measured at 77 K for 1-11 (Figure 8). Complexes with the 298 f8 lowest energy emission maxima, 8-11, and thus the smallest 299 energy gaps between the ground state and lowest ³MLCT state 300 exhibit the highest measured quantum yields of ligand 301 dissociation. This relationship holds true for both experimental 302 emission maxima and calculated E_{00} values obtained from DFT 303 calculations (Table 3, Figures 8 and S26). This relationship 304 shows that the complexes with the lowest energy emission 305 maxima and calculated E_{00} values also have the lowest 306 calculated MSD on the Ru metal center. As previously 307 mentioned, computational results from the Endicott group 308 have suggested that complexes that absorb or emit closer to the 309 NIR region exhibit excited states that tend to possess less CT 310

The Journal of Physical Chemistry C

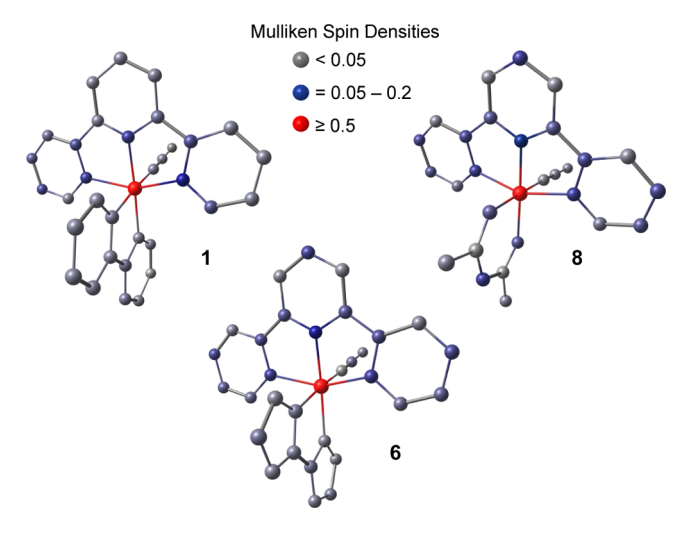


Figure 6. Pictorial representation of the calculated MSDs in the ³MLCT excited state for complexes **1**, **6**, and **8**. The calculated MSD in these three complexes is representative for complexes of the same type (see Figure S25 for other complexes). Hydrogen atoms have been omitted for clarity.

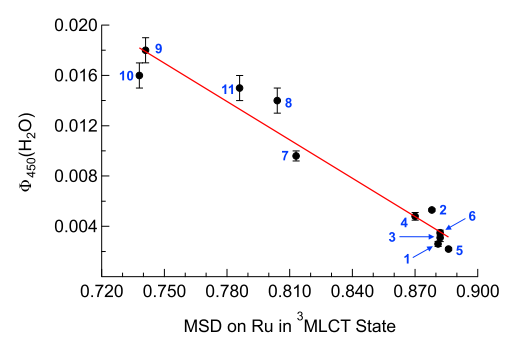


Figure 7. Plot of $\Phi_{450}(H_2O)$ vs calculated MSD on Ru in the ³MLCT excited state for 1–11; the data can be fit to a line with $R^2 = 0.95$.

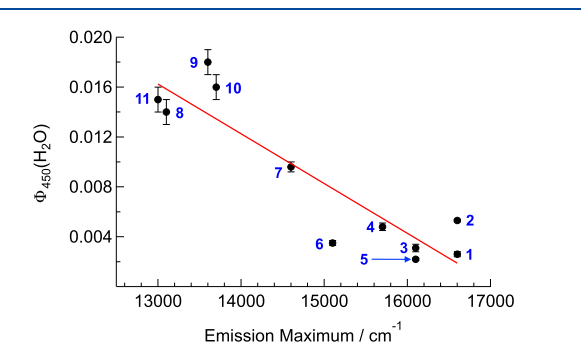


Figure 8. Plot of $\Phi_{450}(H_2O)$ as a function of the emission maximum at 77 K in CH₃CN for 1–11; the data can be fit to a line with $R^2 = 0.83$.

311 character and more ligand-based $\pi\pi^*$ character. One way to 312 red-shift the absorption of these types of Ru(II) complexes is 313 to use electron-rich, donating ligands. These donating ligands 314 raise the energy of the Ru($d\pi$) orbitals closer to the energy of 315 the ligand-based π^* orbitals, thus decreasing the energy of the 316 MLCT transition. This decreased energy gap also allows for a 317 greater degree of mixing between the Ru($d\pi$) and the ligand-318 based π^* orbitals, such that antibonding/bonding molecular 319 orbitals of the mixed metal/ligand character can be formed. 30

donating acac-type ligands, 8-12, show that this model holds $_{321}$ true for the $[Ru(tpy)(L)(CH_3CN)]^{n+}$ series and that the $_{322}$ ancillary ligands can play a significant role in affecting the $_{323}$ character and reactivities of CT states. Previous studies by $_{324}$ Betanzos-Lara and co-workers of Ru—arene complexes have $_{325}$ also shown that the incorporation of electron-donating ligands $_{326}$ enhances ligand photodissociation; however, these studies used $_{327}$ exclusively high-energy ultraviolet or white light irradiation and $_{328}$ offered a limited explanation of the observed differences in $_{329}$ photoreactivity. $_{60}$

The value of $\Phi_{450}(H_2O)$, 0.0012(1), of 12 did not fit the 331 linear relationships in Figures 5, 7, and 8, and is approximately 332 an order of magnitude lower than expected based on the values 333 measured for the acac complex and derivatives, 8-11 (Table 334 3). However, when the photoanation quantum yield of 12 was 335 measured in CH₂Cl₂ solution with 10 mM Bu₄NCl, using the 336 same irradiation wavelength, $\Phi_{450}(Cl) = 0.021(1)$ was 337 recorded (Table 3). This quantum yield is similar to those 338 of 8-11, with $\Phi_{450}(Cl)$ values that range from 0.022(1) to 339 0.027(1) (Table 3). If these photoanation quantum yields are $_{340}$ considered separately, complex 12 now follows the expected 341 trend with percent Ru contribution in the HOMO, MSD on 342 Ru in the ³MLCT state, and emission energy (Figures S27 - 343 S29). These findings are consistent with the lower solubility of 344 the Ru fragment, possessing the hydrophobic DBM ligand 345 following the dissociation of CH₃CN from 12, resulting in 346 recombination with CH₃CN within the solvent cage and lower 347 cage escape to form the aqua product. 59,61 These findings 348 demonstrate that the low $\Phi_{450}(H_2O)$ value of 12 can be 349 attributed to solubility of the product and/or intermediate, 350 pointing to the importance of considering the solubilities of 351 both fragments when designing complexes for efficient ligand 352 photodissociation.

Although the lowest energy ${}^{3}MLCT$ state in 1–12 is Ru(d π) ${}_{354}$ \rightarrow tpy(π^*) in nature, a wide range of photosubstitution 355 reactivity is observed. Therefore, the ancillary bidentate ligand 356 must play a significant role in the photochemistry of these 357 complexes. The spin density on the tpy ligand in the ³MLCT 358 excited state varies only slightly in 1-12 (Table 3), and not 359 with a linear relationship, as is the case with spin density on 360 ruthenium. The ³MLCT state moves electron density from the 361 metal to the tpy ligand. In addition, the bidentate ligand can 362 also be used to further vary the degree of spin density removed 363 from the ruthenium center in the excited state (Table 3). The 364 metal center in the ³MLCT excited state is partially oxidized 365 and is calculated to possess less than one localized unpaired 366 electron in all complexes, 1-12. This decreased electron 367 density on the metal center drastically reduces its ability to π - 368 backbond to the CH₃CN ligand. Because CH₃CN is a 369 relatively poor σ -donor, it relies on back-donation from the 370 metal to form a strong and stable bond, such that Ru-NCCH₃ 371 bond weakening is expected in the ³MLCT excited state. This ₃₇₂ effect is enhanced in complexes with the lowest spin density on 373 the metal, 8-12, further increasing the probability of CH₃CN 374 dissociation. It should be noted, however, that the photo- 375 induced ligand exchange in Ru(II) polypridyl systems with 376 strong σ -donor leaving ligands, such as pyridines or sulfur- 377 coordinated thioethers, 32,62 may occur via a different 378 mechanism, likely through the population of a dissociative 379 ³LF state. ³²⁻³⁶ 380

381 CONCLUSIONS

382 A series of Ru(II) complexes containing the tridentate tpy 383 ligand and various bidentate ancillary ligands were synthesized 384 and evaluated for their ability to dissociate CH₃CN, a model 385 for nitrile-containing drugs, upon irradiation with visible light. 386 The bidentate ligands chosen display a similar degree of steric 387 bulk around the metal center in the ground state, but possess a 388 wide range of electron-donating and electron-withdrawing 389 abilities. Complexes 1-12 display photosubstitution efficien-390 cies that vary by approximately an order of magnitude. The complexes containing the most electron-donating bidentate 392 ligands, 8-11, exhibit the larger quantum yield values for 393 ligand exchange in water. Complexes 8-11 possess the 394 smallest energy gap between the ground state and the lowest 395 energy ³MLCT excited state, and DFT calculations show that a 396 large degree of the ligand character is present in their HOMOs 397 and in their ³MLCT excited states. These results suggest that 398 ligand mixing may affect the back-bonding ability of the metal 399 center in the excited state, increasing the quantum yields of 400 nitrile ligand dissociation. This enhanced reactivity in the excited state is advantageous, as it allows for the design of 402 complexes with greater quantum yields without affecting their 403 thermal stability in the dark. The observed trends between the 404 quantum yield of ligand dissociation and both the MSD on the 405 Ru center in the excited state and the amount of Ru d 406 character in the ground-state HOMO may prove to be useful 407 in the design of new Ru(tpy)-based systems containing nitrile 408 leaving groups.

ASSOCIATED CONTENT

410 S Supporting Information

411 The Supporting Information is available free of charge on the 412 ACS Publications website at DOI: 10.1021/acs.jpcc.9b01576.

Experimental methods, synthetic procedures and characterization data, crystallographic data for 4, 7, and 12, electronic absorption spectra, photolysis spectra and dark controls in H_2O , photoanation relationships, molecular orbitals, and MSDs, and DFT-optimized structures (PDF)

419 AUTHOR INFORMATION

420 Corresponding Authors

421 *E-mail: jrack@unm.edu (J.J.R.).

422 *E-mail: turro.1@osu.edu (C.T.).

423 ORCID ®

424 Jeffrey J. Rack: 0000-0001-6121-879X

425 Claudia Turro: 0000-0003-3202-5870

426 Author Contributions

427 L.M.L. and K.F.A.-A. contributed equally. The manuscript was 428 written through contributions of all authors. All authors have 429 given approval to the final version of the manuscript.

430 Notes

431 The authors declare no competing financial interest.

432 CCDC 1897623-1897625 contains the supplementary 433 crystallographic data for this paper. These data can be

434 obtained free of charge from The Cambridge Crystallographic

435 Data Centre via www.ccdc.cam.ac.uk/structures/.

ACKNOWLEDGMENTS

437 C.T. thanks the National Science Foundation (CHE-1800395) 438 for partial support of this work and the Ohio Supercomputer Center for access to computational resources.⁶³ J.J.R. acknowl- 439 edges the National Science Foundation (grant CHE-1602240) 440 and the University of New Mexico for financial support. 441

REFERENCES

- (1) Thompson, D. W.; Ito, A.; Meyer, T. J. $[Ru(bpy)_3]^{2+}$ and other 443 remarkable metal-to-ligand charge transfer (MLCT) excited states. 444 *Pure Appl. Chem.* **2013**, 85, 1257–1305.
- (2) Shaffer, D. W.; Xie, Y.; Concepcion, J. J. O–O bond formation 446 in ruthenium-catalyzed water oxidation: single-site nucleophilic attack 447 vs O–O radical coupling. *Chem. Soc. Rev.* **2017**, *46*, 6170–6193. 448
- (3) O'Donnell, R. M.; Sampaio, R. N.; Li, G.; Johansson, P. G.; 449 Ward, C. L.; Meyer, G. J. Photoacidic and Photobasic Behavior of 450 Transition Metal Compounds with Carboxylic Acid Group(s). *J. Am.* 451 *Chem. Soc.* **2016**, *138*, 3891–3903.
- (4) Pashaei, B.; Shahroosvand, H.; Graetzel, M.; Nazeeruddin, M. K. 453 Influence of Ancillary Ligands in Dye-Sensitized Solar Cells. *Chem.* 454 *Rev.* **2016**, *116*, 9485–9564.
- (5) Jakubaszek, M.; Goud, B.; Ferrari, S.; Gasser, G. Mechanisms of 456 Action of Ru(II) Polypyridyl Complexes in Living Cells Upon Light 457 Irradiation. *Chem. Commun.* **2018**, *54*, 13040–13059.
- (6) Lemercier, G.; Four, M.; Chevreux, S. Two-Photon Absorption 459 Properties of 1,10-Phenanthroline-based Ru(II) Complexes and 460 Related Functionalized Nanoparticles for Potential Application in 461 Two-Photon Excitation Photodynamic Therapy and Optical Power 462 Limiting. Coord. Chem. Rev. 2018, 368, 1–12.
- (7) Bonnet, S.; Collin, J.-P. Ruthenium-Based Light-Driven 464 Molecular Machine Prototypes: Synthesis and Properties. *Chem.* 465 *Soc. Rev.* **2008**, 37, 1207–1217.
- (8) Mede, T.; Jäger, M.; Schubert, U. S. Chemistry-on-the-Complex: 467 Functional Ru^{II} Polypyridyl-Type Sensitizers as Divergent Building 468 Blocks. *Chem. Soc. Rev.* **2018**, 47, 7577–7627.
- (9) King, A. W.; Wang, L.; Rack, J. J. Excited State Dynamics and 470 Isomerization in Ruthenium Sulfoxide Complexes. *Acc. Chem. Res.* 471 **2015**, 48, 1115–1122.
- (10) Fernández-Moreira, V.; Thorp-Greenwood, F. L.; Coogan, M. 473 P. Application of d⁶ Transition Metal Complexes in Fluorescence Cell 474 Imaging. *Chem. Commun.* **2010**, 46, 186–202.
- (11) Ruggi, A.; van Leeuwen, F. W. B.; Velders, A. H. Interaction of 476 Dioxygen with the Electronic Excited State of Ir(III) and Ru(II) 477 Complexes: Principles and Biomedical Applications. *Coord. Chem.* 478 *Rev.* 2011, 255, 2542–2554.
- (12) Ceroni, P.; Credi, A.; Venturi, M. Light to Investigate (Read) 480 and Operate (Write) Molecular Devices and Machines. *Chem. Soc.* 481 *Rev.* 2014, 43, 4068–4083.
- (13) Barragán, F.; López-Senín, P.; Salassa, L.; Betanzos-Lara, S.; 483 Habtemariam, A.; Moreno, V.; Sadler, P. J.; Marchán, V. Photo- 484 controlled DNA Binding of a Receptor-Targeted Organometallic 485 Ruthenium(II) Complex. J. Am. Chem. Soc. 2011, 133, 14098–14108. 486
- (14) Hammarström, L. Accumulative Charge Separation for Solar 487 Fuels Production: Coupling Light-Induced Single Electron Transfer 488 to Multielectron Catalysis. *Acc. Chem. Res.* **2015**, 48, 840–850.
- (15) Weidmann, A. G.; Komor, A. C.; Barton, J. K. Targeted 490 Chemotherapy with Metal Complexes. *Comments Inorg. Chem.* **2014**, 491 34, 114–123.
- (16) Puntoriero, F.; Serroni, S.; La Ganga, G.; Santoro, A.; Galletta, 493 M.; Nastasi, F.; La Mazza, E.; Cancelliere, A. M.; Campagna, S. 494 Photo- and Redox-Active Metal Dendrimers: A Journey from 495 Molecular Design to Applications and Self-Aggregated Systems. *Eur.* 496 *J. Inorg. Chem.* **2018**, 3887–3899.
- (17) Li, A.; Turro, C.; Kodanko, J. J. Ru(II) Polypyridyl Complexes 498 Derived from Tetradentate Ancillary Ligands for Effective Photo-499 caging. *Acc. Chem. Res.* **2018**, *51*, 1415–1421.
- (18) White, J. K.; Schmehl, R. H.; Turro, C. An Overview of 501 Photosubstitution Reactions of Ru(II) Imine Complexes and Their 502 Application in Photobiology and Photodynamic Therapy. *Inorg. Chim.* 503 *Acta* 2017, 454, 7–20.

- 505 (19) Li, A.; Turro, C.; Kodanko, J. J. Ru(ii) polypyridyl complexes as 506 photocages for bioactive compounds containing nitriles and aromatic 507 heterocycles. *Chem. Commun.* **2018**, *54*, 1280–1290.
- 508 (20) Yip, A. M.-H.; Lo, K. K.-W. Luminescent rhenium(I), 509 ruthenium(II), and iridium(III) polypyridine complexes containing 510 a poly(ethylene glycol) pendant or bioorthogonal reaction group as 511 biological probes and photocytotoxic agents. *Coord. Chem. Rev.* **2018**, 512 *361*, 138–163.
- 513 (21) Chan, H.; Ghrayche, J. B.; Wei, J.; Renfrew, A. K. Photolabile 514 Ruthenium(II)-Purine Complexes: Phototoxicity, DNA Binding, and 515 Light-Triggered Drug Release. *Eur. J. Inorg. Chem.* **2017**, 1679–1686. 516 (22) Luis, E. T.; Iranmanesh, H.; Beves, J. E. Photosubstitution 517 Reactions in Ruthenium(II) Trisdimine Complexes: Implications for 518 Photoredox Catalysis. *Polyhedron* **2019**, 160, 1–9.
- 519 (23) Kosgei, G. K.; Breen, D. J.; Lamb, R. W.; Livshits, M. Y.; 520 Crandall, L. A.; Ziegler, C. J.; Webster, C. E.; Rack, J. J. Controlling 521 Photoisomerization Reactivity Through Single Functional Group 522 Substitutions in Ruthenium Phosphine Sulfoxide Complexes. *J. Am.* 523 Chem. Soc. 2018, 140, 9819–9822.
- 524 (24) Rachford, A. A.; Rack, J. J. Picosecond Isomerization in 525 Photochromic Ruthenium—Dimethyl Sulfoxide Complexes. *J. Am.* 526 Chem. Soc. **2006**, 128, 14318—14324.
- 527 (25) Matsui, J. K.; Lang, S. B.; Heitz, D. R.; Molander, G. A. 528 Photoredox-Mediated Routes to Radicals: The Value of Catalytic 529 Radical Generation in Synthetic Methods Development. *ACS Catal.* 530 **2017**, *7*, 2563–2575.
- 531 (26) Colasson, B.; Credi, A.; Ragazzon, G. Light-Driven Molecular 532 Machines Based on Ruthenium(II) Polypyridine Complexes: 533 Strategies and Recent Advances. *Coord. Chem. Rev.* **2016**, 325, 534 125–134.
- 535 (27) Yeung, M. C.-L.; Yam, V. W.-W. Molecular Design of Novel 536 Classes of Luminescent Transition Metal Complexes and Their Use in 537 Sensing, Biolabeling, and Cell Imaging. *Struct. Bonding* **2014**, *165*, 538 109–129.
- 539 (28) Juris, A.; Balzani, V.; Barigelletti, F.; Campagna, S.; Belser, P.; 540 Von Zelewsky, A. Ru(II) polypyridine complexes: photophysics, 541 photochemistry, eletrochemistry, and chemiluminescence. *Coord.* 542 *Chem. Rev.* 1988, 84, 85–277.
- 543 (29) Thomas, R. A.; Tsai, C. N.; Mazumder, S.; Lu, I. C.; Lord, R. 544 L.; Schlegel, H. B.; Chen, Y. J.; Endicott, J. F. Energy Dependence of 545 the Ruthenium(II)-Bipyridine Metal-to-Ligand-Charge-Transfer Ex-546 cited State Radiative Lifetimes: Effects of $\pi\pi^*$ (bipyridine) Mixing. *J.* 547 *Phys. Chem. B* **2015**, *119*, 7393–7406.
- 548 (30) Odongo, O. S.; Allard, M. M.; Schlegel, H. B.; Endicott, J. F. 549 Observations on the Low-Energy Limits for Metal-to-Ligand Charge-550 Transfer Excited-State Energies of Ruthenium(II) Polypyridyl 551 Complexes. *Inorg. Chem.* **2010**, *49*, 9095–9097.
- 552 (31) Lord, R. L.; Allard, M. M.; Thomas, R. A.; Odongo, O. S.; 553 Schlegel, H. B.; Chen, Y.-J.; Endicott, J. F. Computational Modeling 554 of the Triplet Metal-to-Ligand Charge-Transfer Excited-State 555 Structures of Mono-Bipyridine-Ruthenium(II) Complexes and 556 Comparisons to Their 77 K Emission Band Shapes. *Inorg. Chem.* 557 **2013**, 52, 1185–1198.
- 558 (32) Knoll, J. D.; Albani, B. A.; Turro, C. New Ru(II) Complexes for 559 Dual Photoreactivity: Ligand Exchange and $^{1}O_{2}$ Generation. *Acc.* 560 Chem. Res. **2015**, 48, 2280–2287.
- 561 (33) Knoll, J. D.; Turro, C. Control and Utilization of Ruthenium 562 and Rhodium Metal Complex Excited States for Photoactivated 563 Cancer Therapy. *Coord. Chem. Rev.* **2015**, 282–283, 110–126.
- 564 (34) Howerton, B. S.; Heidary, D. K.; Glazer, E. C. Strained 565 Ruthenium Complexes as Potent Light-Activated Anticancer Agents. 566 J. Am. Chem. Soc. 2012, 134, 8324–8327.
- 567 (35) Wacholtz, W. M.; Auerbach, R. A.; Schmehl, R. H.; Ollino, M.; 568 Cherry, W. R. Correlation of Ligand Field Excited-State Energies with 569 Ligand Field Strength in (Polypyridine)Ruthenium(II) Complexes. 570 *Inorg. Chem.* 1985, 24, 1758–1760.
- 571 (36) Wagenknecht, P. S.; Ford, P. C. Metal Centered Ligand Field 572 Excited States: Their Roles in the Design and Performance of

- Transition Metal Based Photochemical Molecular Devices. Coord. 573 Chem. Rev. 2011, 255, 591–616.
- (37) Tfouni, E. Photochemical Reactions of Ammineruthenium(II) 575 Complexes. Coord. Chem. Rev. 2000, 196, 281–305.
- (38) Tfouni, E.; Ford, P. C. Thermal and Photochemical Properties 577 of Some Trans-Disubstituted Tetraammineruthenium(II) Complexes 578 of Aromatic Nitrogen Heterocycles, *trans*-Ru(NH₃)₄LL'ⁿ⁺. *Inorg.* 579 *Chem.* 1980, 19, 72–76.
- (39) Malouf, G.; Ford, P. C. Photochemical Reaction Pathways of 581 Ru(II) Complexes. Evidence Regarding the Reactive Excited State(s) 582 from Metal-to-Ligand Charge Transfer Excitation of Pentamine- 583 (pyridine)ruthenium(2+) and Related Complexes. J. Am. Chem. Soc. 584 1974, 96, 601–603.
- (40) Sun, Q.; Mosquera-Vazquez, S.; Lawson Daku, L. M.; Guénée, 586 L.; Goodwin, H. A.; Vauthey, E.; Hauser, A. Experimental Evidence of 587 Ultrafast Quenching of the ³MLCT Luminescence in Ruthenium(II) 588 Tris-bipyridyl Complexes via a ³dd State. *J. Am. Chem. Soc.* **2013**, *135*, 589 13660–13663.
- (41) Knoll, J. D.; Albani, B. A.; Durr, C. B.; Turro, C. Unusually 591 Efficient Pyridine Photodissociation from Ru(II) Complexes with 592 Sterically Bulky Bidentate Ancillary Ligands. *J. Phys. Chem. A* **2014**, 593 118, 10603–10610.
- (42) Knoll, J. D.; Albani, B. A.; Turro, C. Excited State Investigation 595 of a New Ru(II) Complex for Dual Reactivity with Low Energy Light. 596 *Chem. Commun.* **2015**, *51*, 8777–8780.
- (43) Wachter, E.; Heidary, D. K.; Howerton, B. S.; Parkin, S.; 598 Glazer, E. C. Light-Activated Ruthenium Complexes Photobind DNA 599 and are Cytotoxic in the Photodynamic Therapy Window. *Chem.* 600 *Commun.* 2012, 48, 9649–9651.
- (44) van Rixel, V. H. S.; Siewert, B.; Hopkins, S. L.; Askes, S. H. C.; 602 Busemann, A.; Siegler, M. A.; Bonnet, S. Green Light-Induced 603 Apoptosis in Cancer Cells by a Tetrapyridyl Ruthenium Prodrug 604 Offering Two *Trans* Coordination Sites. *Chem. Sci.* **2016**, 7, 4922—605 4929.
- (45) Bonnet, S.; Collin, J.-P.; Sauvage, J.-P.; Schofield, E. 607 Photochemical Expulsion of the Neutral Monodentate Ligand L in 608 Ru(tpy*)(diimine)(L)²⁺: A Dramatic Effect of the Steric Properties of 609 the Spectator Diimine Ligand. *Inorg. Chem.* **2004**, *43*, 8346–8354. 610
- (46) Laemmel, A.-C.; Collin, J.-P.; Sauvage, J.-P. Efficient and 611 Selective Photochemical Labilization of a Given Bidentate Ligand in 612 Mixed Ruthenium(II) Complexes of the Ru(phen)₂L²⁺ and Ru- 613 (bipy)₂L²⁺ Family (L = Sterically Hindering Chelate). *Eur. J. Inorg.* 614 *Chem.* 1999, 383–386.
- (47) Loftus, L. M.; Li, A.; Fillman, K. L.; Martin, P. D.; Kodanko, J. 616 J.; Turro, C. Unusual Role of Excited State Mixing in the 617 Enhancement of Photoinduced Ligand Exchange in Ru(II) Com- 618 plexes. J. Am. Chem. Soc. 2017, 139, 18295–18306.
- (48) Nakamura, G.; Kondo, M.; Crisalli, M.; Lee, S. K.; Shibata, A.; 620 Ford, P. C.; Masaoka, S. Syntheses and Properties of Phosphine- 621 Substituted Ruthenium(II) Polypyridine Complexes with Nitrogen 622 Oxides. *Dalton Trans.* **2015**, 44, 17189–17200.
- (49) Ross, H. B.; Boldaji, M.; Rillema, D. P.; Blanton, C. B.; White, 624 R. P. Photosubstitution in Tris Chelate Complexes of Ruthenium(II) 625 Containing the Ligands 2,2'-Bipyrizine, 2,2'-Bipyrimidine, 2,2'- 626 Bipyridine, and 4, 4'-Dimetly-2,2'-bipyridine: Energy Gap Control. 627 Inorg. Chem. 1989, 28, 1013–1021.
- (50) Malouf, G.; Ford, P. C. Photochemistry of the Ruthenium(II) 629 Ammine Complexes, $Ru(NH_3)_5(py-X)^{2+}$. Variations of Systemic 630 Parameters to Modify Photochemical Reactivities. *J. Am. Chem. Soc.* 631 **1977**, 99, 7213–7221.
- (51) Avci, P.; Gupta, A.; Sadasivam, M.; Vecchio, D.; Pam, Z.; Pam, 633 N.; Hamblin, M. R. Low-Level Laser (Light) Therapy (LLLT) in 634 Skin: Stimulating, Healing, Restoring. Semin. Cutaneous Med. Surg. 635 **2013**, 32, 41–52.
- (52) Barolet, D. Light-Emitting Diodes (LEDs) in Dermatology. 637 Semin. Cutaneous Med. Surg. 2008, 27, 227–238. 638
- (53) Cherry, W. R.; Henderson, L. J., Jr. Relaxation Processes of 639 Electronically Excited States in Polypyridine Ruthenium Complexes. 640 *Inorg. Chem.* **1984**, 23, 983–986. 641

- 642 (54) Medlycott, E. A.; Hanan, G. S. Synthesis and Properties of 643 Mono- and Oligo-Nuclear Ru(II) Complexes of Tridentate Ligands:
- 644 The Quest for Long-Lived Excited States at Room Temperature. 645 Coord. Chem. Rev. 2006, 250, 1763-1782.
- 646 (55) Loftus, L. M.; Al-Afyouni, K. F.; Turro, C. New Ru^{II} Scaffold 647 for Photoinduced Ligand Release with Red Light in the Photo-
- 648 dynamic Therapy (PDT) Window. *Chem.—Eur. J.* **2018**, 24, 11550—649 11553.
- 650 (56) Rasmussen, S. C.; Ronco, S. E.; Mlsna, D. A.; Billadeau, M. A.;
- 651 Pennington, W. T.; Kolis, J. W.; Petersen, J. D. Ground- and Excited-
- 652 State Properties of Ruthenium(II) Complexes Containing Tridentate 653 Azine Ligands, $Ru(tpy)(bpy)L^{2+}$, Where L Is a Polymerizable
- 654 Acetylene. *Inorg. Chem.* **1995**, 34, 821–829. 655 (57) Tsai, C.-N.; Allard, M. M.; Lord, R. L.; Luo, D.-W.; Chen, Y.-I.;
- 656 Schlegel, H. B.; Endicott, J. F. Characterization of Low Energy
- 657 Transfer Charge Transfer Transitions in (Terpyridine)(Bipyridine)-
- 658 Ruthenium(II) Complexes and Their Cyanide-Bridged Bi- and Tri-659 Metallic Analogues. *Inorg. Chem.* **2011**, *50*, 11965–11977.
- 660 (58) Hecker, C. R.; Fanwick, P. E.; McMillin, D. R. Evidence for
- 661 Dissociative Photosubstitution Reactions of (Acetonitrile)-
- 662 (Bipyridine)(Terpyridine)Ruthenium(2+). Crystal and Molecular
- 663 Structure of [Ru(tpy)(bpy)(py)](PF₆)₂·(CH₃)₂CO. *Inorg. Chem.* 664 **1991**, 30, 659–666.
- 665 (59) Rohrabaugh, T. N., Jr.; Xue, K. A.; White, J. K.; Kodanko, J. J.;
- 666 Turro, C.; Turro, C. New Ru(II) Complex for Dual Photo-
- 667 chemotherapy: Release of Cathepsin K Inhibitor and ¹O₂ Production. 668 *Dalton Trans.* **2018**, 47, 11851–11858.
- 669 (60) Betanzos-Lara, S.; Salassa, L.; Habtemariam, A.; Nováková, O.;
- 670 Pizarro, A. M.; Clarkson, G. J.; Liskova, B.; Brabec, V.; Sadler, P. J.
- 671 Photoactivatable Organometallic Pyridyl Ruthenium(II) Arene
- 672 Complexes. Organometallics **2012**, 31, 3466–3479.
- 673 (61) Lampe, F. W.; Noyes, R. M. Absolute Quantum Yields for 674 Dissociation of Iodine in Inert Solvents. *J. Am. Chem. Soc.* 1954, 76,
- 675 2140-2144.
- 676 (62) Jang, H. J.; Hopkins, S. L.; Siegler, M. A.; Bonnet, S. Frontier
- 677 Orbitals of Photosubstitutionally Active Ruthenium Complexes: An 678 Experimental Study of the Spectator Ligands' Electronic Properties
- 679 Influence on Photoreactivity. *Dalton Trans.* **2017**, *46*, 9969–9980.
- 680 (63) Ohio Supercomputer Center. Owens Supercomputer; Ohio
- 681 Supercomputer Center: Columbus, OH, 2016. http://osc.edu/682 ark:19495/hpc6h5b1.